3

Borehole geophysical methods

J.L. Mari

Surface geophysical methods are stand-alone methods which enable the construction of a 2D or 3D geophysical model of the subsurface link to one or more physical parameters, such as resistivity for MT or EM methods, seismic wave velocities and density for seismic methods. Geological surveys associated with surface geophysical surveys lead to build a structural geological model to detect heterogeneities or tectonic features such fractures or faults. Such models are used to define the location of boreholes.

Drilling of a borehole gives geophysicists the opportunity to perform borehole geophysical measurements and record additional data.

Borehole geophysical methods give borehole measurements used to validate and calibrate geophysical models, to convert in depth geophysical models obtained in time (as example time migrated seismic sections in depth sections), to transform geophysical models in physical or petrophysical models. As example, seismic models in amplitude are converted into velocity models and then into porosity models. Borehole geophysical methods provide high-resolution, localized information on properties like lithology, porosity, and fluid content.

Borehole geophysical methods can be classified as conventional logging methods, borehole surface imaging methods, hydrogeological logging methods, full

DOI: https://doi.org/10.1051/978-2-7598-3752-6.c003

waveform acoustic logging and borehole seismic methods. We present examples of some borehole geophysical methods and applications.

For more and detail information, we recommend reading specific books in well logging (Boyer and Mari, 1997; Serra and Serra, 2000; Chapellier, 2001a,b among others) and borehole seismic (Hardage, 1985, 1992; Mari et Vergniault, 2018 among others), as well as specific magazines, as “*The log analyst* “.

3.1 Conventional logging methods

The logging tools currently run are calipers, natural radioactivity tool (natural gamma ray GR), electric resistivity and electric conductivity tools (laterologs and induction) with shallow or large depth investigation, induced radioactivity tools (neutron and density), dipmeters and acoustic tools. The logs have a vertical and horizontal resolution of several tens of cm.

Well logs are recorded to identify the different geological formations crossed by a borehole. Using the response equations of logging tools and after correction for environmental effects, it is possible to obtain the physical parameters of a geological formation such as the resistivity R_t of the virgin zone, the neutron porosity ΦN, the slowness Δt (inverse of the propagation velocity), the density ρ_b.

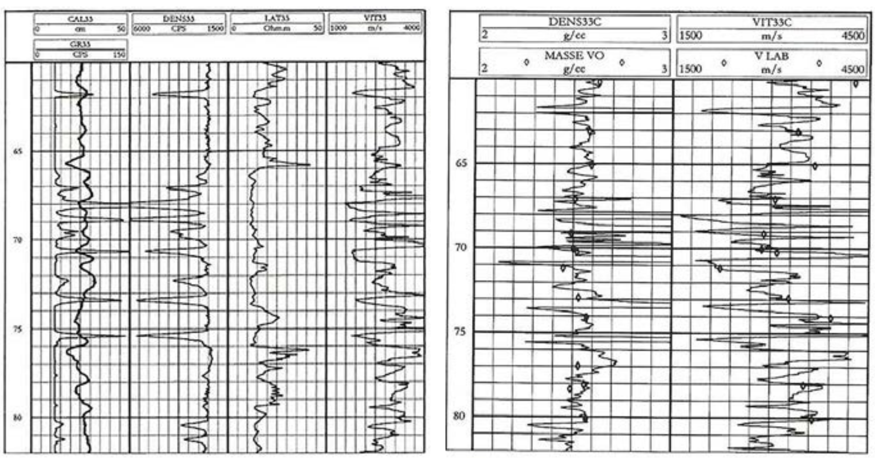

(a) (b)

Figure 3.1 *Example of logs recorded in an altered formation (after Chapellier, in Mari et al., 1999). (a) Caliper (CAL33), gamma ray (GR33), density (DENS33), Resistivity (laterolog LAT33), slowness Δt converted in velocity VIT33). (b) Comparison between core measurements and density and velocity logs after environmental corrections*

Quick look or sophisticated quantitative interpretation methods (Boyer and Mari, 1997) based on relationships between measured physical parameters and petrophysical parameters are used to obtain petrophysical (such as porosity) and mechanical (such as Poisson's ratio) parameters of geological formations.

Figure 3.1 is an example of logs recorded in the molasse of the Swiss Plateau. The geological formation, constituted of argillaceous sandstone, is strongly altered.

The caliper shows numerous caved zones in shaly beds (Figure 3.1a) strongly marked on the density and velocity logs. After correcting the logs according to the caliper, the logs are not perfect, but the values are close to those obtained on cores (Figure 3.1b).

Archie (1942) has shown empirically that for water-saturated permeable formations, the relation between the true formation resistivity, R_t, and the resistivity, R_w, of the water impregnating the formation is given by:

$$R_t/R_w = F = \Phi^{-m} \tag{3.1}$$

where F is the "resistivity formation factor". Φ is proportional to the formation porosity and m is a "cementation factor", that is a formation characteristic. An approximate value equal to 2 is generally adopted for the cementation factor.

Wyllie et al. (1956) has established a linear relationship between the slowness Δt and the porosity Φ and shalyness V_{sh} of a water-saturated permeable formation:

$$\Delta t = (1 - \Phi - V_{sh})\Delta t_{ma} + V_{sh}\Delta t_{sh} + \Phi \cdot \Delta t_f \tag{3.2}$$

where ma, sh and f represent respectively the matrix, the shales and the fluid.

The same relationships are used for the neutron porosity ΦN and the density ρ_b.

$$\Phi N = (1 - \Phi - V_{sh})\Phi N_{ma} + V_{sh}\Phi N_{sh} + \Phi \cdot \Phi N_f \tag{3.3}$$

$$\rho_b = (1 - \Phi - V_{sh})\rho_{ma} + V_{sh}\rho_{sh} + \Phi \cdot \rho_f \tag{3.4}$$

Logs are also recorded to add constraints in the processing and interpretation of geophysical models.

The University of Poitiers (France) has developed a Hydrogeological Experimental Site (HES) for the sole purpose of providing facilities to perform long-term monitoring and experiments for a better understanding of fluid flow and transfers in fractured rocks (Bourbiaux et al., 2007). 35 boreholes, including two vertical and two inclined cored boreholes, were drilled on the site in two separate campaigns: 2002-2003 and 2004 (Figure 3.2a). All the boreholes are crossing completely the Dogger Aquifer (depth of boreholes = 125 m). A 3D survey has been designed to obtain a 3D interval velocity cube in depth (Mari and Porel, 2007). Figure 3.2b shows the resistivity log recorded in borehole M09 as well as the velocity distribution extracted from the 3D velocity block at the location of borehole M09.

Faust (1953) has established an empirical relationship between seismic velocity V, depth Z, and electrical resistivity measurements Rt. For a formation of a given lithology, the velocity V can be written as a function of the depth Z and resistivity R_t as follows:

$$V = C \cdot (Z \cdot R_t)^{1/b} \tag{3.5}$$

with:

- V the P-wave velocity of the formation in m/s,
- Z the depth in m,
- R_t the electrical resistivity in Ω·m,
- C and b the coefficients associated with Faust's equation.

At each well where a long normal log has been recorded, an interval velocity log has been extracted from the 3D seismic interval velocity block. The two sets of data (resistivity and seismic velocity) have been combined to calibrate an empirical Faust's law, which has then been used as a local constraining function to transform the 3D pseudo-velocity block into a 3D pseudo-resistivity block. For each well, the two coefficients, C (constant coefficient) and b (power law exponent), of that empirical law were determined through a least-square minimization of the difference between the 3D-block-extracted seismic velocities and the velocities predicted from Faust's law using the long normal resistivity log data as input. The previous seismic-derived 3D resistivity block (R_t-seis) was converted into a 3D pseudo-porosity block, by using the Archie-law-derived formula (equation (3.1) with m = 2). The results are shown in Figures 3.2c and 3.2d. Figure 3.2c shows the long normal resistivity log R_t, the resistivity log R_t-seis converted from seismic velocity log using Faust's law, the estimated seismic porosity log using Archie's law. Figure 3.2d shows porosity and velocity sections extracted from the 3D blocks, oriented South-East North-West, and passing close to borehole M09. The high porosity layer, observed on the porosity log at 87 m depth (Figure 3.2c) clearly appears on the porosity section in the 45–100 m interval distance (Figure 3.2d).

The example shows how long normal resistivity logs can be used as constraints to transform seismic velocity sections into seismic sections in porosity, using petrophysical equations established by Faust and Archie.

In addition to conventional logging tools, borehole wall imaging tools, such as formation micro scanner, high resolution acoustic or optical televiewers are currently run. The tools provide high resolution (several cm) oriented images of the borehole walls. They are used to detect dips, discontinuities, features such as fractures, to show diameter changes with open fractures and breakouts. They are also used to identify facies and perform stratigraphic interpretations (Gaillard et al., 2024).

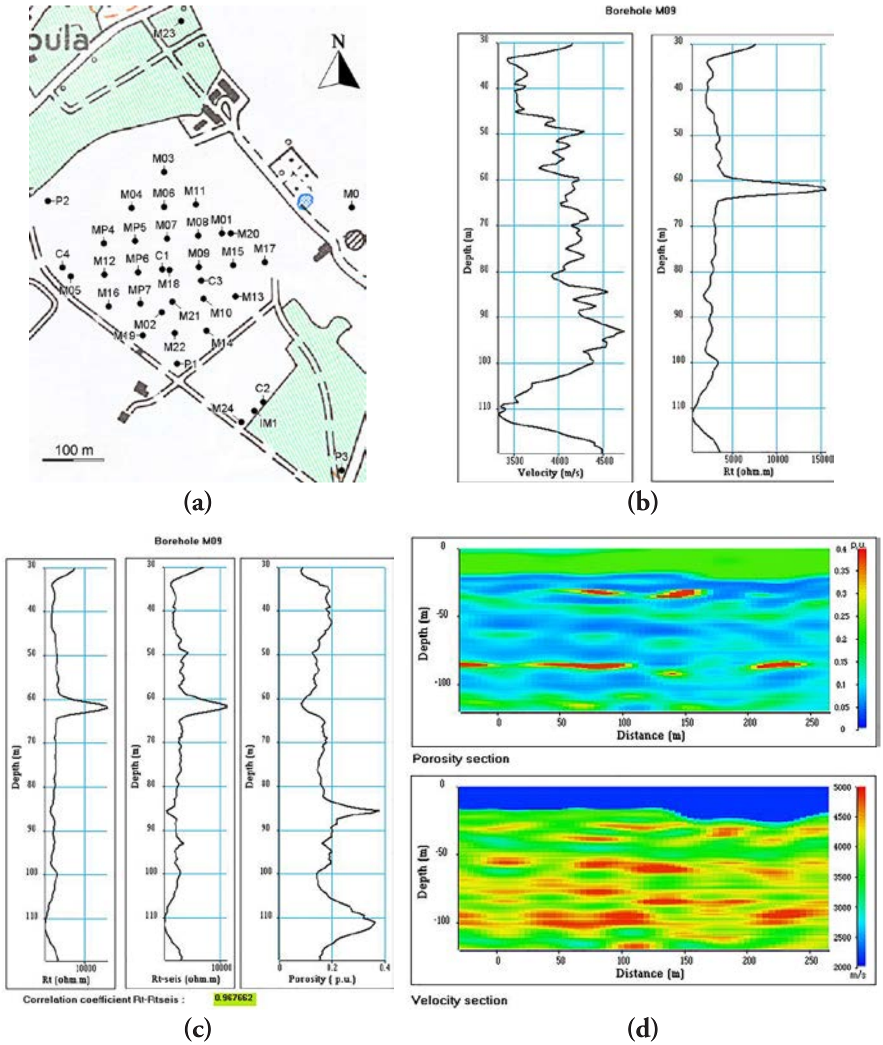

Figure 3.2 *Seismic velocity to porosity transforms using long normal resistivity logs and Faust's law. (a) Borehole location, (b) seismic velocity log and log normal resistivity log at borehole M09, (c) long normal resistivity log R_t, resistivity log R_t-seis converted from seismic velocity log using Faust's law, estimated seismic porosity log using Archie's law, (d) porosity and velocity seismic sections.*

3.2 Hydrogeological methods

Conventionally, hydrogeological investigations concern hydraulic measurements such as flows and temperature. They also concern hydraulic testing such slug test and pumping test (Mari et Porel, 2024).

A GFTC logger records logs which show the evolution of the Gamma radiation (G), the water velocity (F), the water temperature (T) and the electrical conductivity of the water (C) as a function of depth.

Temperature logs are carried out in wells to detect any anomalies linked to water intakes in the borehole. Figure 3.3a shows temperature logs recorded in wells M8 and M13 of the HES (Figure 3.2a). For well M8, the temperature increases steadily with the depth. The increase is consistent with the regional geothermal gradient, which is about 2.5 degrees per 100 meters. For well M13, the temperature log shows abrupt variations about 60 and 85 meters deep. These variations are likely related to water intake.

Recording the vertical velocity of the water makes it possible to determine the direction of flow circulation in a borehole (upward or downward flow). The type of experimentation can be carried out under static conditions or in dynamic conditions, either by pumping in the monitored well, or by pumping in a well offseted from the well being monitored. The experiment makes it possible to know precisely the depths of the producing levels. Figure 3.3b shows an example of flowmeter test performed in M07 well with pumping in M06. The flow log shows a downward flow between 35 and 88 meters, where the flow enters the formation, also visible both on temperature and conductivity logs.

A slug test is a particular type of aquifer test where water is quickly added or removed from a groundwater well, and the change in hydraulic head is monitored through time, to determine the near-well aquifer characteristics. Figure 3.4 is an example of a slug test carried out on the well M19 (Figure 3.2a). The changes in hydraulic head versus time observed on the nearby wells (M16, P1, MP7, M22, MP6, M21) are displayed in Figure 3.4a.

The slug test shows that wells MP7 and P1 are not directly connected to well M19. On the other hand, well MP6 shows oscillations due to the injection of water into M19. MP21 and MP22 seem to be strongly connected to M19. By repeating these operations on various wells of the experimental site, a map of connectivity between wells can be elaborated as shown in Figure 3.4b.

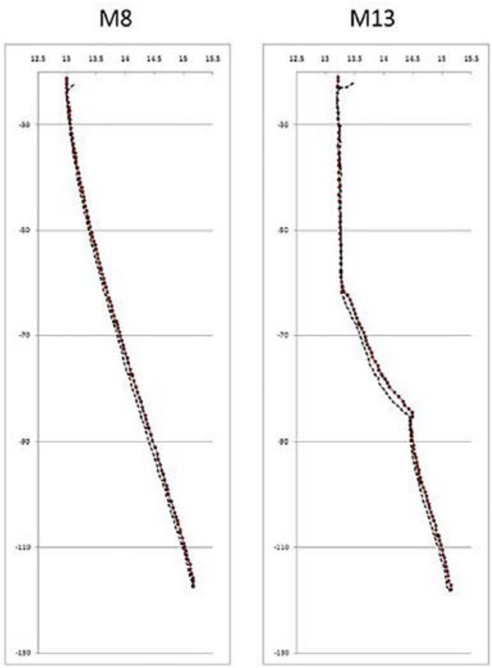

(a)

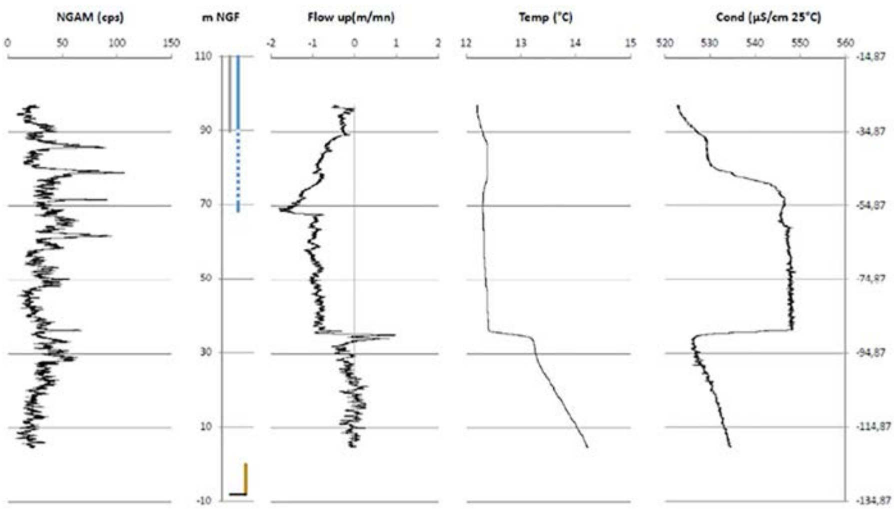

(b)

Figure 3.3 *Examples of GFTC logs (after Mari and Porel, 2024). (a) Temperature logs, (b) flow log obtained under dynamic condition in borehole M07 with pumping in M06 well (from left to right: gamma ray, flowmeter, temperature, conductivity observed in M07 well).*

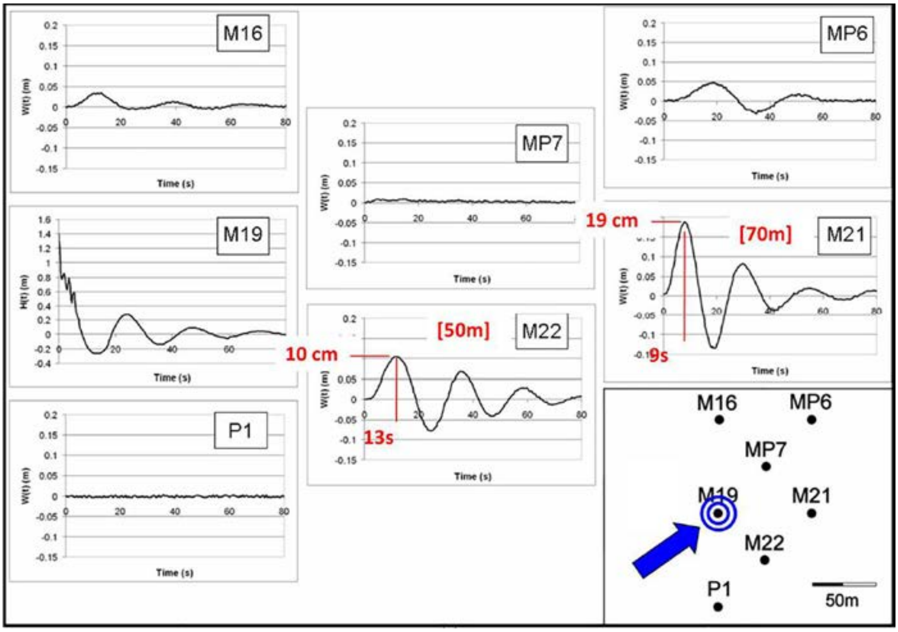

(a)

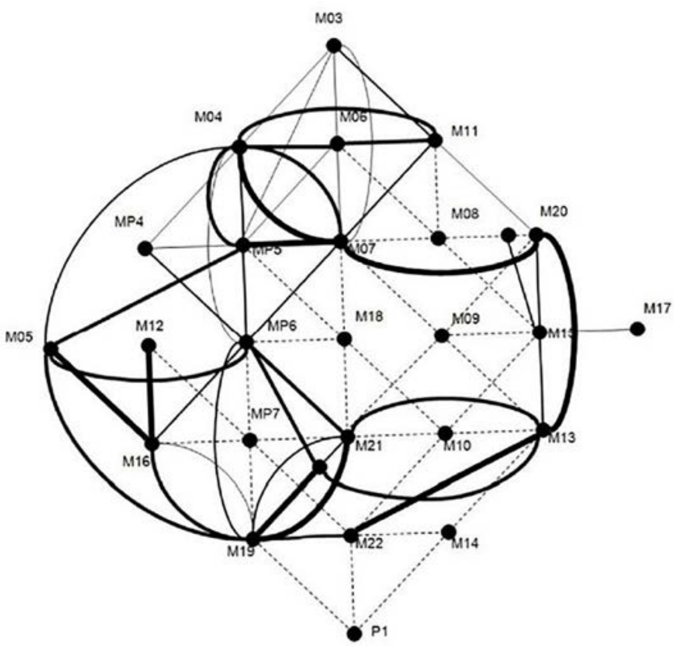

(b)

Figure 3.4 *Example of slug test (a) and connectivity map (b) (after Mari and Porel, 2024).*

3.3 Full waveform acoustic methods

Acoustic tools are currently run to measure velocities (P-wave velocity VP, S-wave velocity VS) of geological formations. The tools used are of monopole or dipole type. Monopole-type tools are the most used. For monopole tools, sources and receivers are multidirectional. In the fluid, sources generate a compression wave which creates in the formation a compression wave (P wave) and a shear wave (S wave) at the refraction limit angles. Dipole tools are used to access the shear velocity (VS) of geological formations and are equipped with polarized transmitters and receivers. Such tools generate polarized compression waves perpendicular to the well axis. The compression waves create flexure modes at the well wall which generate in the formation pseudo-shear waves propagating parallel to the well axis.

Acoustic tools are built with one source (multidirectional) and 2 receivers (multidirectional) at least, or several sources (multidirectional and polarized) and several receivers (multidirectional and polarized). Acoustic tools are working in wide frequency bandwidths: 1–40 kHz for monopole tool and 1–3 kHz for dipole tool. Consequently, the sampling rates are of several µs in time (5 or 10 µs for monopole tool, 20 µs for dipole tool) and of several centimetres in depth (5 to 30 cm). Full waveform acoustic measurements can be represented as constant-offset sections. A constant-offset section is a set of acoustic records represented as a function of depth and obtained with a fixed source-to-receiver distance.

In a vertical well, monopole tools can enable the recording of five propagation modes as: refracted compression waves (P), refracted shear waves (S, only in fast formations VS > VP fluid, P-wave velocity of the borehole fluid), fluid waves (F), and two dispersive guided modes as pseudo-Rayleigh waves (in fast formations), and Stoneley waves (ST). The acoustic logs associated with the different waves are very high-resolution logs and can be compared with core measurements. The acoustic logs currently obtained for each type of wave are velocity or slowness logs, frequency and attenuation logs.

In addition to these modes, constant-offset acoustic sections may show coherent slanted events and resonances (R). The slanted events, conventionally named criss-cross events, are refracted events reflected on the edges of geological discontinuities (acoustic impedance discontinuities), such as fractures. For their part, the resonances are related to poor cementation between the casing and the formation. A high level of resonances can result in unusable acoustic data.

Figures 3.5 to 3.8 show an example of acoustic data recorded in boreholes situated on an experimental site located in the Cher region (France) at the transition from Triassic to Jurassic geological formations, partly overlaid by thin superficial formations. The sedimentary formation is mainly composed of limestone up to 120 m depth and sandstones with some argillite and dolomite intercalations between 120 m and 200 m.

The site was investigated from the surface via hybrid seismic imaging methods and from two boreholes (B1 and B2, Figure 3.5a) via FWAL and VSP (Mari et al., 2021, 2023, 2024). A seismic line was recorded at the site with a seismic spread composed of 48 fixed geophones (2 m lag distance between neighbors,

Figure 3.5a), while the source, as a weight dropper (Figure 3.5a), was moved and fired in the middle of all pairs of adjacent geophones. Hybrid seismic imaging combining refraction (tomography, Figure 3.5a) and reflection seismic results produced an extended depth reflectivity section starting from the surface up to a depth of 240 m (Figure 3.5b). Time to depth conversion was calculated using the time-depth law given by the VSP recorded in borehole B1 (Mari et al., 2021). The site was also investigated by a near surface 3D seismic survey (Mari and Mendes, 2019: see Figures 2.27 to 2.29, chapter 2).

Borehole B1 was drilled to a depth of 80 m and equipped with a cemented steel casing. Borehole B2 was drilled in two drilling phases. In the first phase, B2 was drilled to a depth of 120 m and equipped with cemented steel casing to a depth of 78 m. B2 remains in open hole between 78 and 120 m. In the second phase, B2 was drilled to a depth of 192 m and equipped with a slotted PVC casing in the 78–120 m depth interval. Resonances observed on constant offset acoustic sections reveals that B1 is a poorly cemented case hole (Figure 3.6) and B2 is an uncemented cased hole up to 78 m, B2 being equipped with an uncemented slotted PVC casing from 78 m to 192 m depth.

The acoustic tool used for field experiments is a monopole-type flexible tool with a small diameter of 50 mm. It holds a magnetostrictive transmitter (transmission frequencies: 17–22 kHz) and can be equipped with two pairs of piezoelectric receivers offering an acquisition in near offset configuration (receivers at 1 and 1.25 m beneath the source), and in far offset configuration (receivers 3 and 3.25 m beneath the source).

Figures 3.6 and 3.7 shows a comparison between acoustic data recorded using the tool in the near (or short) offset configuration (receivers at 1 and 1.25 m from the source) and in the far (or large) offset configuration (receivers at 3 and 3.25 m).

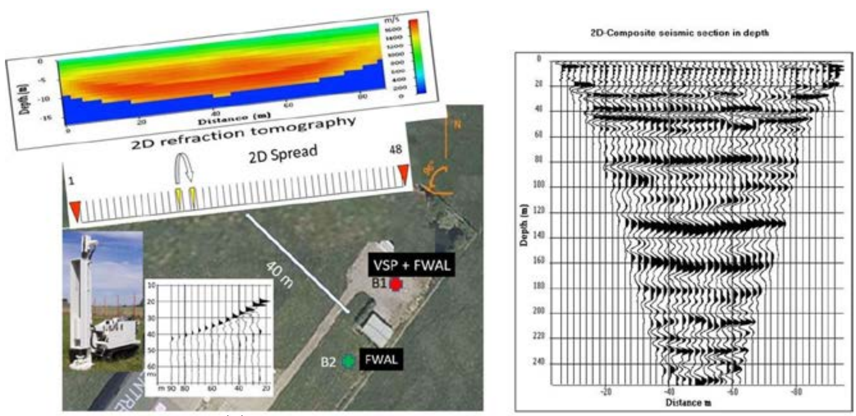

(a) (b)

Figure 3.5 *Seismic imaging: (a) 2D seismic spread – 2D refraction tomography, borehole locations (B1 and B2), view of the seismic source, VSP recorded in B1, (b) 2D hybrid section over depth (after Mari et al., 2021).*

In borehole B1 (Figure 3.6) which is poorly cemented resulting in strong resonances, the short-offset configuration (1 m) only shows refracted P-waves in the 60–70 m depth interval. In contrast, the large offset is less sensitive to resonances, letting clearly appear refracted P-waves along the profile. For both offsets, the differentiation between the refracted P-waves (P) and the Stoneley waves (ST) can be done easily.

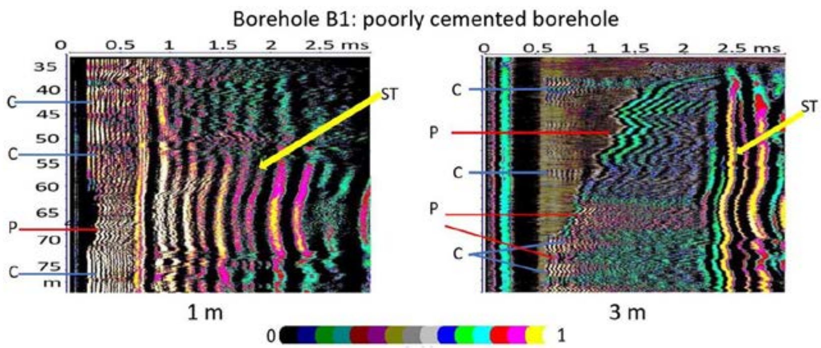

Figure 3.6 *Comparison of short offset (1 m) and large offset (3 m) acoustic sections recorded in borehole B1 (poorly cemented borehole). The different wave trains are identified by letters: C casing resonances, P refracted P-wave, ST Stoneley wave. The acoustic sections are normalized and displayed with a color scale ranging from 0 to 1 (after Mari et al., 2023).*

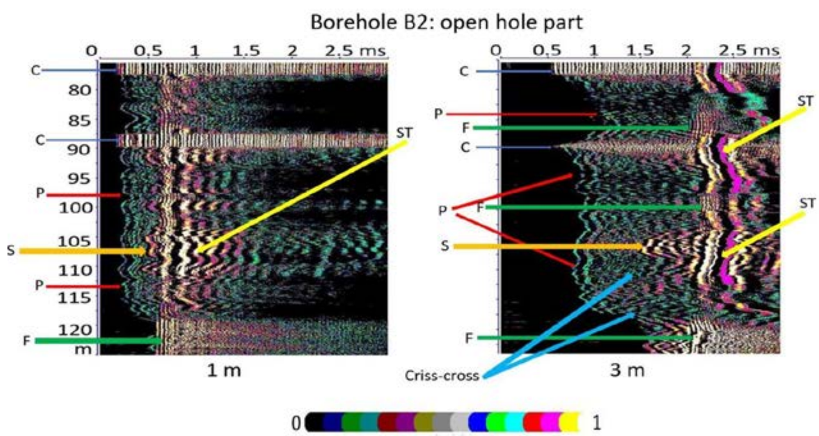

Figure 3.7 *Comparison of short offset (1 m) and large offset (3 m) acoustic sections recorded in the open hole part of borehole B2. The different wave trains are identified by letters: C casing resonances, P refracted P-wave, S converted refracted S-wave, F fluid wave, ST Stoneley wave, criss-cross. The acoustic sections are normalized and displayed with a color scale ranging from 0 to 1 (after Mari et al., 2023).*

In the open hole part of borehole B2 (Figure 3.7), the presence of a piece of casing generates resonances in the depth interval 88–91 m on the 1 m offset section. The influence of the piece of casing is local on the 3 m offset section, indicating that the length of the piece of casing is a slightly larger than 3 m. On the 1m offset section, it is possible to identify the refracted P-waves, locally the converted refracted S waves, the Stoneley modes and the fluid modes. With a short-offset configuration, the different wave trains can interfere. However, we can notice that a large offset (3 m) better separates the different wave trains over time due to the difference in their propagation velocities. On the 3 m offset section, criss-cross events are visible.

The short-offset configuration must be favored to evaluate the borehole cementation. For measurements of wave parameters such as amplitude, frequency content, propagation velocity, a large offset configuration must be favored.

Full waveform acoustic data, recorded with the large offset configuration (3 and 3.25 m), in borehole B1 (steel cased hole) in the 30–78 m depth interval and in borehole B2 (slotted PVC cased hole) in the 78–192 m depth interval are merged to obtain composite acoustic sections. Figure 3.8 (right side) shows the composite acoustic section with an offset of 3 m. The acoustic data were processed to obtain a very high-resolution velocity log (Figure 3.8) which was converted in pseudo porosity log using the Raymer equation adapted to carbonate formation (Raymer et al., 1980). The porosity log was then used

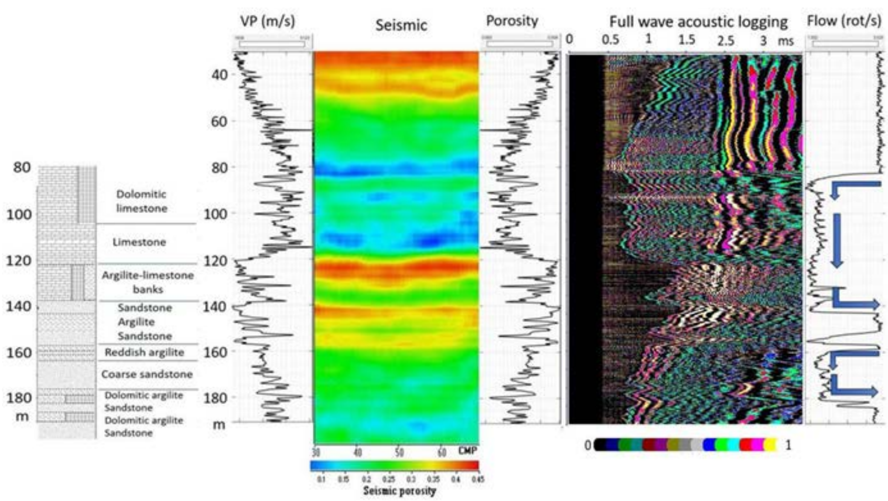

Figure 3.8 *Seismic imaging and full waveform acoustic logging: from left to right: lithological column, acoustic velocity, seismic section converted in porosity, acoustic porosity, Full wave acoustic composite section (0–80 m: borehole B1, 80–190 m: borehole B2 slotted PVC cased hole) and flowmeter. The acoustic section is normalized and displayed with a color scale ranging from 0 to 1 (after Mari et al., 2021).*

as a constraint to transform the seismic section into pseudo-porosity section. The results are shown within the 30–190 m depth interval in Figure 3.8, with high-porosity layers appearing in red (Mari et al., 2021). The pseudo porosity section, associated with a flowmeter recorded in the slotted PVC part of borehole B2, informs on preferential areas where flows occur. Levels of in-flows or out-flows, indicated by blue arrows on the flowmeter, clearly show two flow loops, completely independent over depth (83–143 m and 159–181 m depth intervals).

With full waveform data, provided by multi-source and multi-receiver logging tools, recorded in deviated or horizontal boreholes, it is possible to conduct a well micro seismic survey based on the analysis of modes reflected and diffracted on acoustic impedance discontinuities within formations or at formation boundaries. Processing of reflected modes leads to depth migrated acoustic sections with very high resolution (a few tens of centimeters) providing an image with a depth of investigation of several meters from the well trajectory (Hirabayashi et al., 2024).

Hirabayashi et al. (2024) shows an example of depth migrated acoustic section obtained in a highly deviated geothermal well with a sonic tool consisting of 13 receiver stations spaced at 0.1524-m intervals, each with eight azimuthal receivers. The minimum distance between source and receivers is 3.795 m, and a dipole chirp source was used during data acquisition. Figure 3.9a shows depth migration images above and below the actual borehole trajectory indicated by the black curve. Parallel reflectors dipping down to the right by about 3º are consistently observed. Figure 3.9b shows a zoomed image for the black box shown in Figure 3.9a. Stratigraphic structures (of approximately 10º dip) are observed within a potential geothermal reservoir, with the reflector at ~1634 m vertical depth corresponding to the base of an oolite dune.

Full waveform acoustic logging has a very good vertical resolution (a few decimeters). Its lateral investigation with respect to the borehole is of a few centimeters for interface dispersive modes, a few tens of centimeters for refracted modes and a few meters for reflected modes (less than 20 meters).

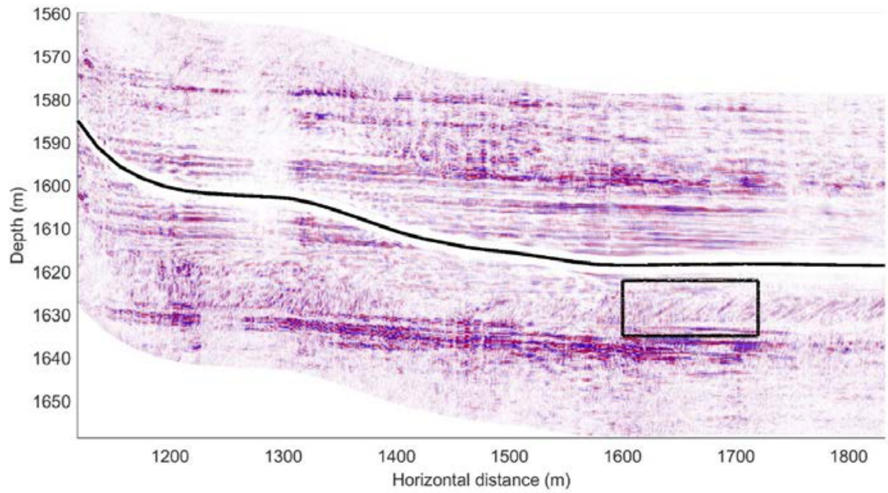

(a)

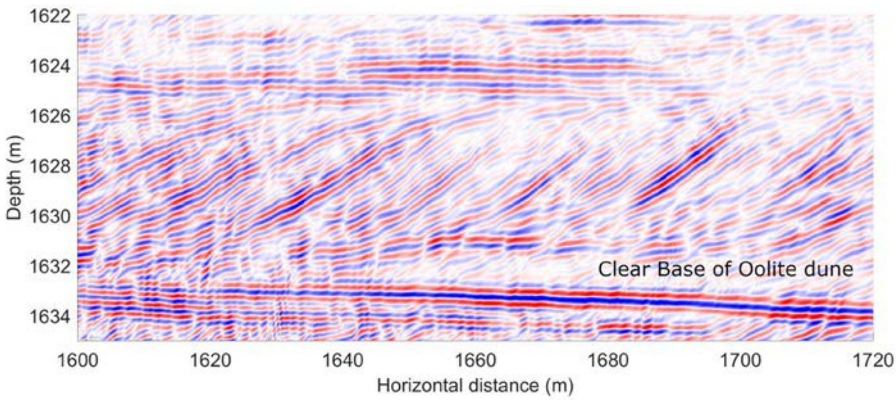

(b)

Figure 3.9 *Depth migrated acoustic section obtained in a highly deviated geothermal well (after Hirabayashi et al., 2024). Depth migration image and borehole geometry in the vertical depth (a). Enlargement of the 120 m (long) × 13 m (high) rectangle window shown in a, which shows noiseless, highly defined geological progradations (b).*

3.4 Borehole seismic method

Vertical Seismic Profile or VSP (Hardage 1985, 1992; Mari et al., 1999; Mari and Coppens, 2003; Mari and Vergniault, 2018) is the most used form of well seismic surveying conducted in vertical wells. VSP is a well seismic method for which the source and the receiver are approximatively on the same vertical. The VSP vertical resolution ranges from meters to tens of meters and its lateral range of investigation can reach a few tens of meters (Fresnel zone). After processing, a VSP provides a seismic trace, that is directly comparable to a surface seismic section recorded in the vicinity of the well.

The lateral range of investigation of a VSP is increased by doing acquisition in deviated wells or can be improved by offsetting the source with respect to the well in case of vertical well. This technique is called Offset Vertical Seismic Profiling (OVSP). The image obtained after processing is thus a single-fold seismic section. A Seismic Walkaway is a series of offset VSPs, with the surface source situated at several locations corresponding to successively increasing offsets with respect to the borehole. The image obtained after processing is a section with a low degree of multiple fold coverage.

For VSP acquisition, the sources are vibrators or weight droppers for on-shore surveys, air guns or sparkers for off-shore surveys. The borehole sensor can be a single-component geophone (vertical geophone) or a three-component geophone (a vertical component and two orthogonal horizontal components). The borehole sensor can also be a hydrophone, or even a four-component sensor: a three-component geophone and a hydrophone. The receiver can also be a string of borehole sensors, allowing the acquisition of data at several depth levels simultaneously (between 4 and 12 levels). Distributed Acoustic Sensing (DAS) is an established technology for recording seismic response using optical fiber cables (Willis, 2022). The DAS technology is being used with increasing success in VSP, especially due to the selective sensitivity of the fiber to axial deformations. Mestayer et al. (2011), Mateeva et al. (2013, 2014), Lesnikov and Allanic (2014) demonstrated that DAS data provides VSP results comparable with conventional VSP acquisition. However, current DAS systems have a much higher noise floor than geophones meaning that small events may be harder to detect (Baird et al., 2024). DAS technology can be deployed in high temperature, highly deviated or horizontal wells. Meantime the current limitations of the DAS VSP are also well known. Directivity pattern, attenuation of the signal with the length of the fiber cable, uncertainty of the depth determination are among the observed problems (Lesnikov and Allanic, 2014). DAS VSP recorded with fiber cable, which can be deployed behind casing (Didraga, 2015) or production tubing, can provide a much denser spatial sampling than a geophone string at a relatively low cost per sensor.

A VSP record is a two-dimensional record, with a vertical axis which represents the recording time and the horizontal axis which represents the depth locations of the borehole sensor. In case of vertical well, the horizontal axis is the vertical depth expressed in m. In case of deviated well, it represents the cable length. The borehole deviation must be measured and considered in the processing sequence. The frequency content of well seismic data, being generally wider (up to 150–175 Hz) than that of surface seismic data, the time sampling interval does not exceed 2 ms (between 0.5 to 2 ms). The distance between 2 adjacent sensor locations must be chosen to be less than the smallest half-wavelength encountered to avoid spatial aliasing phenomenon (Mari, 2015), usually between 5 and 20 m. For Offset VSP or seismic walkaway acquisition, the offset D of the source relative to the wellhead depends on the depth H of the objective. An offset D < 3/4 H allows to obtain VSP sections, with reflected events for which angles of incidence do not exceed 30 degrees, recommended for amplitude analysis versus angle or offset.

For a VSP recorded in a vertical well, crossing geological layers with small dips, wave field, emitted by a source located at a small offset from the well head, propagates at normal incidence. In these conditions, if the seismic source generates P-waves, VSP records are composed of down-going and up-going P-waves and Stoneley waves. There is no phenomenon of conversion from P-wave to shear wave (S-wave). The P-wave field is composed of primary waves and multiples. Stoneley waves, more commonly known as tube waves, are created when the particles of the sludge column that fills the well are set in motion. Surface waves are the main source of tube waves, which are considered as organized noises that disrupt VSP recordings. However, tube waves, created by conversion of P-wave, are very useful to detect layers of high permeability. In case of wave propagation at normal incidence, VSP can be recorded using a vertical geophone or a hydrophone.

Figure 3.10 is an example of VSP recorded with a vertical geophone and a hydrophone, in a reconnaissance borehole of about 400 m depth drilled to determine the geothermal parameters of the geological formations crossed, as part of a deep

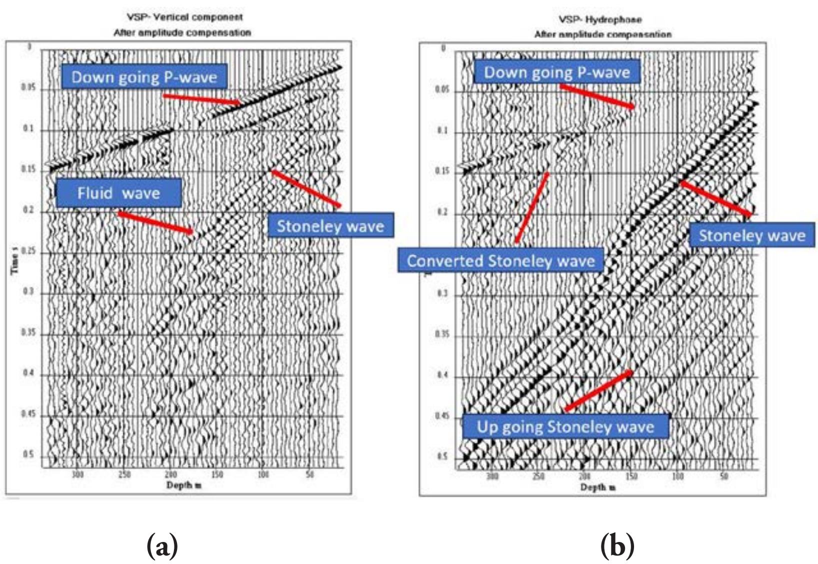

Figure 3.10 *VSP sections (a: vertical geophone, b: hydrophone) and wave identification (After Mari et al., 2024).*

geothermal project, in southern Luxembourg. The VSP was recorded with a depth sampling interval of 5 m in the 20–330 m depth interval. The source is a vibrating source emitting a sweep in the 20–120 Hz frequency band. The offset of the source from the borehole head is 8 m. The time sampling interval is 0.5 ms. Figure 3.10 shows the VSP sections, after amplitude compensation, observed on the vertical geophone and on the hydrophone. On the vertical geophone section, we observe a downgoing P-wave, strongly attenuated in the 150–200 m depth interval. We note the presence of both a downgoing Stoneley wave attenuated from 150 m and a fluid wave (with a propagation velocity of 1540 m/s) in the 150–200 m depth interval. On the hydrophone section, we observe the downgoing P-wave with a conversion to a Stoneley wave at a depth of about 200 m. We also observe a strong downgoing Stoneley wave with a set of reflected upgoing Stoneley waves, the strongest of which occurs at the depth where the converted downgoing Stoneley wave is created

The processing sequence includes amplitude recovery, picking of the arrival times of downgoing wave fields, wave separation of downgoing and upgoing waves, both for P-wave and Stoneley wave. Figure 3.11a shows the extraction of dogoing and upgoing P-waves. Picking of the arrival times of the downgoing wave fields (P-wave and Stoneley wave) is used to compute time versus depth laws (Figure 3.11b), interval velocity logs, and attenuation logs after flattening of the downgoing wave fields (Figure 3.12).

The reconnaissance borehole crosses, after a few meters of landfill and alluvium, that is unconformably underlain by rather similar mainly marly formations dating from the Upper and Middle Liassic, showing slight facies changes towards more silty and sandy or more calcareous facies (units lo4 to lo1a and lm3 to lm1; Toarcian to Pliensbachian, Lower Jurassic).

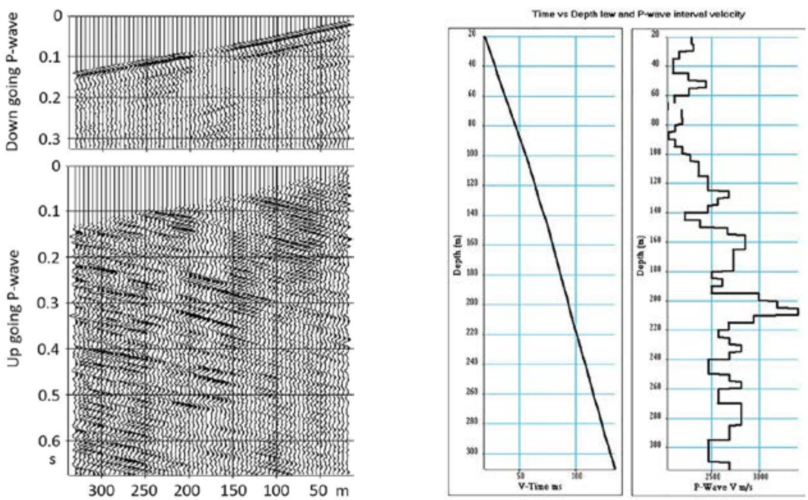

(a) **(b)**

Figure 3.11 *VSP vertical geophone processing: Down going and up going P-wave separation (a), Time versus depth law and P-wave interval velocity log (b) (after Mari et al., 2024).*

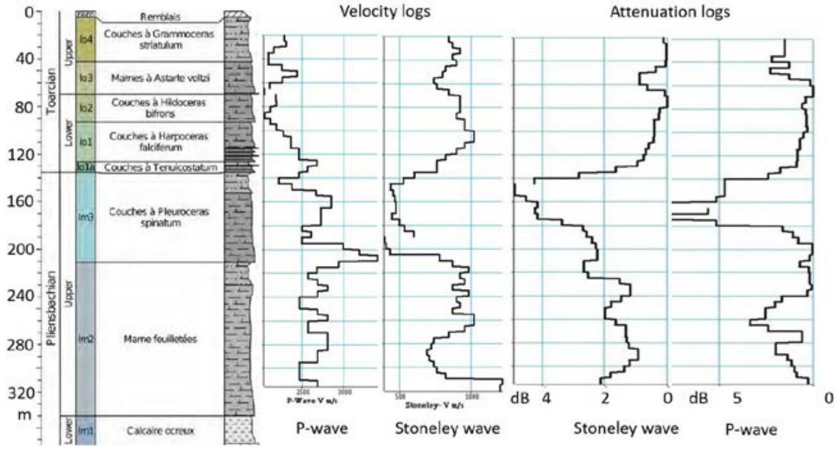

Figure 3.12 *Lithology and VSP logs: velocity and attenuation logs (after Mari et al., 2024).*

In detail, the lithology record by the Geological Survey shows, after the 2 rather homogeneously marly units lo4 and lo3, a gradually increasing content in organic matter, observed in the lo2 and lo1 units (70–126 m), also showing a thin lamination, culminating in the lo1a unit below (126–139 m), which is more silty, sandy and contains bituminous horizons. Below, the lm3 unit appears to have an even higher sand/silt content but is also richer in limestone nodules and beds (140–210 m). The following lm2 unit, the sand and silt content gradually decreases again until the depth of 230 m and the basis of this unit (at 340 m) is homogeneously marly. We note a significant decrease in shear velocity in the 140–200 m depth interval corresponding to the lo1a and lm3 units, richer in sand/silt and organic matter (lo1a) or limestone (lm3). Figure 3.12 (on the right) shows the attenuation logs computed from the downgoing P and Stoneley waves. The results obtained (decrease of both energy and velocity of the Stoneley wave) are consistent with the results which could be obtained by a Biot-Rosenbaum model (Rosenbaum, 1974) used to access to permeability from the evolution of Stoneley's phase velocity and attenuation (Mari, 1989). The velocity and attenuation VSP logs show a very good correspondence with respect to the lithological variations observed in the borehole (Figure 3.12).

The well was equipped with a hybrid cable, comprising 2 optical fibers and 2 electrical conductors, suitable for geothermal applications. Fiber optic temperature measurement enables optimal monitoring of temperature distribution and thermal conductivity in the subsurface as a function of depth. Temperature measurements are made before and after heat injection phases, which are carried out by sending an electric current through the electrical conductors of the hybrid cable. Before heat injection, the temperature increases linearly from 12 °C at 20 m to 23 °C at 320 m (Figure 3.13).

Once the heat injection phase has begun, temperature profiles, recorded after different heating time intervals, show the evolution of the subsurface temperature after respectively 1 h (cyan curve), 3 h (yellow curve) and 108 h (red curve) of thermal

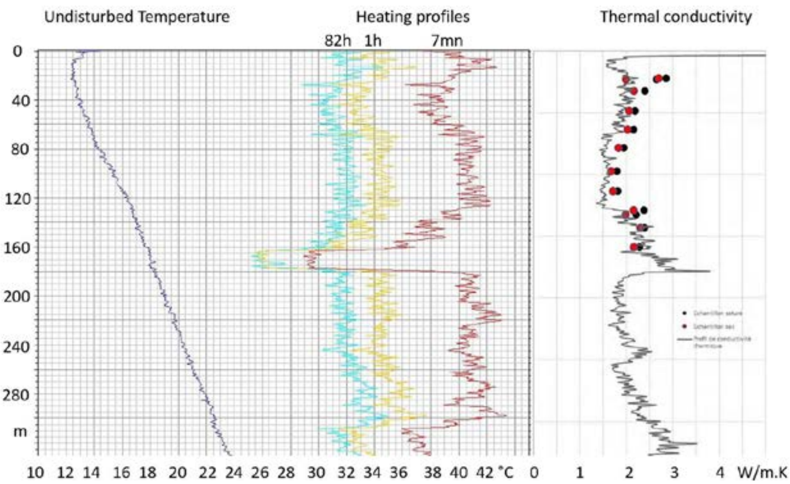

Figure 3.13 *Geothermal tests. Service géologique du Luxembourg document.*

dissipation (Figure 3.13). Different variations, similar on each of the curves, can be identified during the heat injection phase. The main anomaly, located between 160 and 180 m deep, results in a smaller increase in temperature compared to the surrounding depths. Based on the lithologic description the occurrence of a higher sand/silt, organic matter or limestone content observed in the units lo1a and lm3 can be identified at the depths corresponding to these anomalies with lower temperature increases. These can therefore be interpreted as a due to a higher groundwater flow rate in the facies having a slightly higher permeability, causing a leaching of the thermal plume. The heat supplied is more efficiently dissipated thanks to this flow, resulting in a smaller rise in temperature.

The presence of flows is confirmed by Stoneley wave velocity decrease (Figure 3.12), Stoneley wave and P-wave attenuation increase (Figure 3.14) and the presence of a fluid wave (Figure 3.10) in the 140–180 m depth interval. We also note a good correspondence between the thermal conductivity profile (Figure 3.13) and the attenuation VSP logs (Figure 3.14).

The conventionnal processing sequence of a VSP includes amplitude recovery, picking of the arrival times of downgoing wave fields, wave separation using both f-k filters and SVD (singular value decomposition) filters (Mari, 2015), deconvolution of upgoing P-wave fields by the associated downgoing P-wave fields, design of stacking corridor on flattened deconvolved upgoing P-wave section and computation of corridor stacked traces in time. Figures 3.15 and 3.16 ilustrate the processing sequence of a near surface VSP recorded in borehole B1 of the experimental site located in the Cher region (Figure 3.5a). The borehole sensor is an anchored vertical geophone. The source is a weight drop (Figure 3.5a).

The VSP is acquired in the 25 to 90 m depth interval, with a depth sampling interval of 5 m (Figure 3.15a). The listening time is 250 ms. The time sampling interval is 0.25 ms.

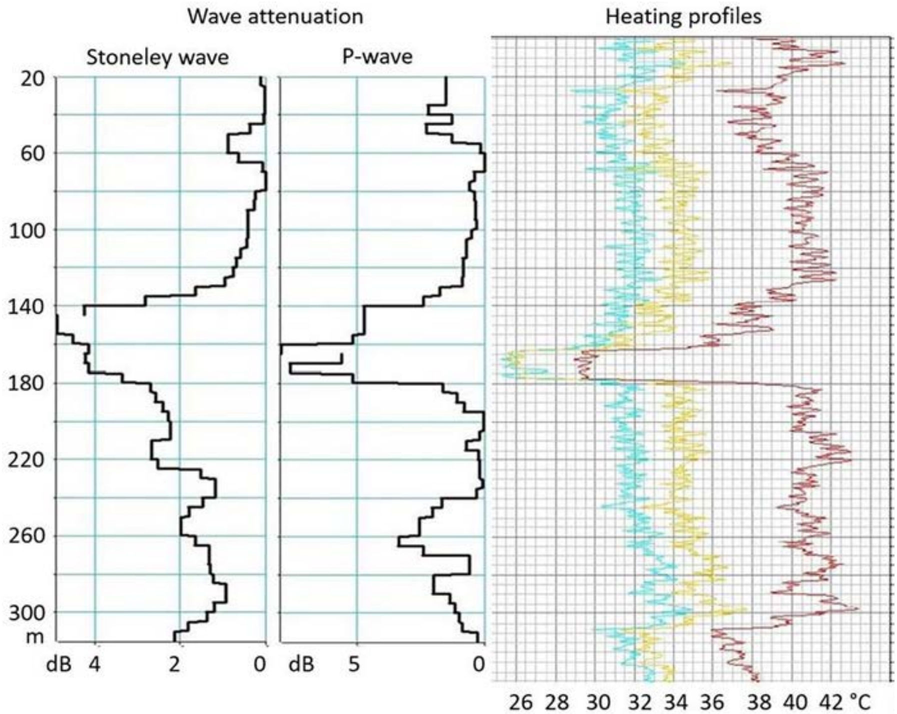

Figure 3.14 *Wave attenuation versus heating profiles (after Mari et al., 2024).*

The picked times of the first arrivals (downgoing P-waves) are used to compute the time versus depth law and the P-wave interval velocity log (Figure 3.15b). The upgoing and downgoing P-waves are separated by an f-k filter (Figures 3.15c and 3.15d). After deconvolution, the upgoing wave field is flattened (Figure 3.16a), a stacking corridor section is designed and a corridor stacked trace is computed (Figure 3.16b). The VSP trace stacked in a corridor (corridor stacked trace or VSP stacked trace), which represents the reflectivity function filtered in the seismic bandwidth and associated with the geological medium crossed by the borehole, is used to calibrate seismic sections located in the vicinity of borehole B1. The corridor stacked trace is used to identify primary reflections on surface seismic sections. For that purpose, the corridor stacked trace duplicated several times is inserted in a seismic section at the location of borehole B1 (Figures 3.16c and 3.16d). In the example, the seismic section is extracted from the 3D block, obtained by a 3D survey conducted on the site (Mari and Mendes, 2019: see Figures 2.27 to 2.29, chapter 2). Another approach is to use both velocity log obtained by acoustic logging (Figure 3.7, right side) and density log to compute synthetic seismograms (SS). The VSP stacked traces (indicated by a red rectangle) and the synthetic seismograms (indicated by a blue rectangle) are inserted in the 3D seismic section. The results are shown both in time and depth (Figures 3.16c and 3.16d), after depth conversion using the time versus depth conversion law (Figure 3.15b). The synthetic seismogram enables the identification of reflectors in the depth range where the logs have been recorded. The VSP stacked trace allows the identification in the same depth range, but it also enables the prediction of reflectors under the well, particularly in the 90 to 140 m range.

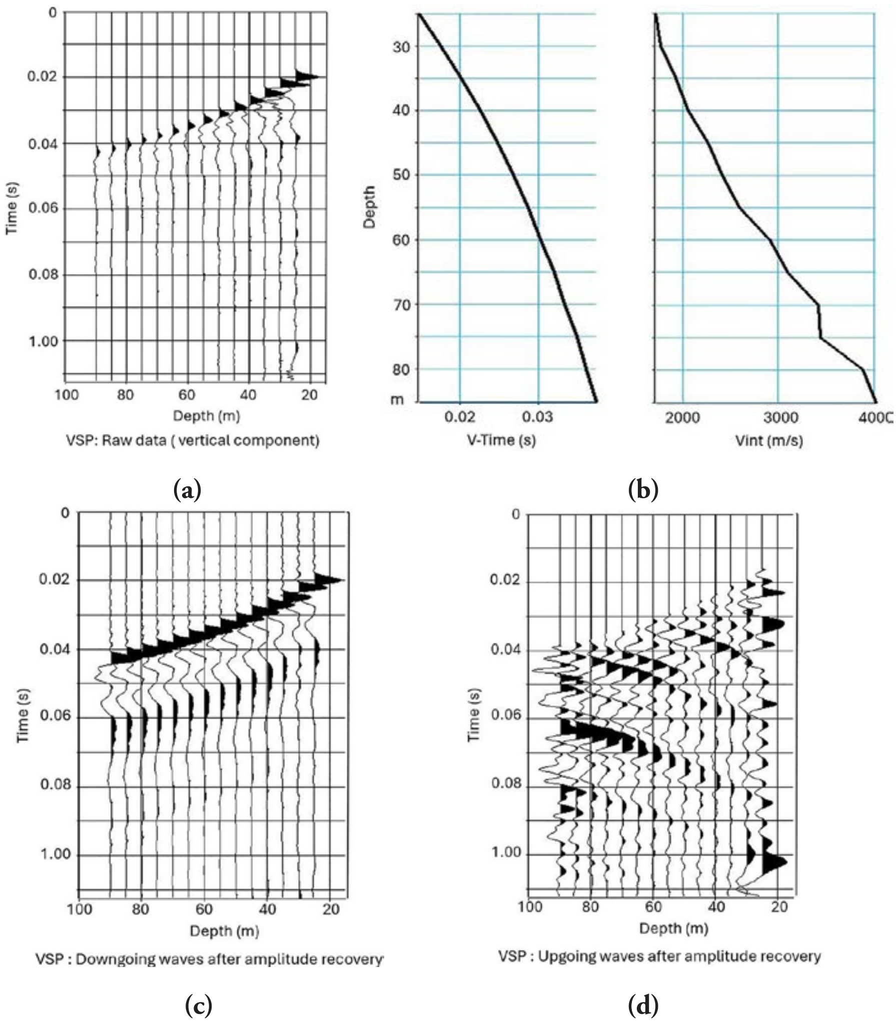

Figure 3.15 *Processing of a near surface VSP, after Mari and Vergniault (2018). (a) Raw data, (b) vertical time and interval velocities, (c) downgoing P-waves, (d) P-upgoing waves.*

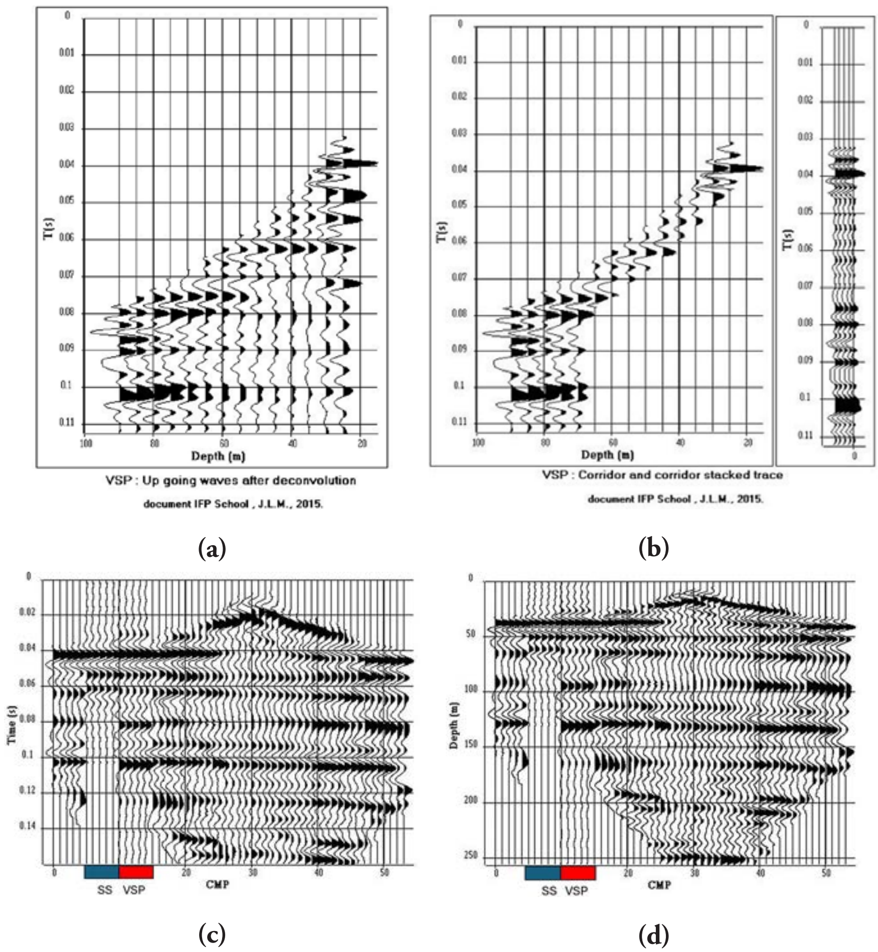

Figure 3.16 *Processing of a near surface VSP, after Mari and Vergniault (2018). (a) Deconvolved upgoing P-waves, (b) stacking corridor and stacked trace; (c) and (d) seismic section, VSP stacked trace and synthetic seismogram in time (c) and in depth (d).*

In case of acquisition of wave fields that do not propagate at normal incidence, it is recommended the use of 3-component borehole sensors to record the different wave trains, in particular the waves converted from P to S. Wave propagation at not normal incidence occurs in acquisition of:

- VSP in boreholes drilled in complex geological structures (dips and faults),
- VSP in deviated wells,
- Offset VSP and walkaway.

Considering the trajectory of the well and the fact that the borehole sensor can rotate from one depth to another, the 3 components (X, Y, Z) of the sensor must be oriented using either hardware orientation device or algorithms based on the analysis of wave polarizations used to define rotation angles for orientation (Naville, 2024). Figures 3.17 and 3.18 are an example of a 3C VSP orientation in a deviated well (Kazemi, 2009). After rotations, the oriented components are defined as follows: Z-component (ZV) is vertical pointing downward, X-component (HN) is horizontal pointing to North and Y-component (HE) is horizontal pointing the East true geographic direction.

After orientation, the 3C VSP processing sequence (Hardage, 1985; Mari and Coppens, 2003; Serbutoviez et al., 2003) includes wave separation with apparent velocity filter and polarization filters (Mars et al., 1999) to extract P and S-waves and separate downgoing and upgoing waves, deconvolution of the upgoing wave fields (P and S waves) by a single operator extracted from the downgoing wave fields, normal moveout correction of deconvolved upgoing waves and stack in CMP gather, or prestack migration in time or depth. The most used method is the VSP -CDP stack method proposed by Wyatt and Wyatt (1982). The VSP migrated seismic section is directly comparable to a surface reflection seismic section. The VSP migrated section has a lateral range of investigation of a few tens to a few hundreds of meters.

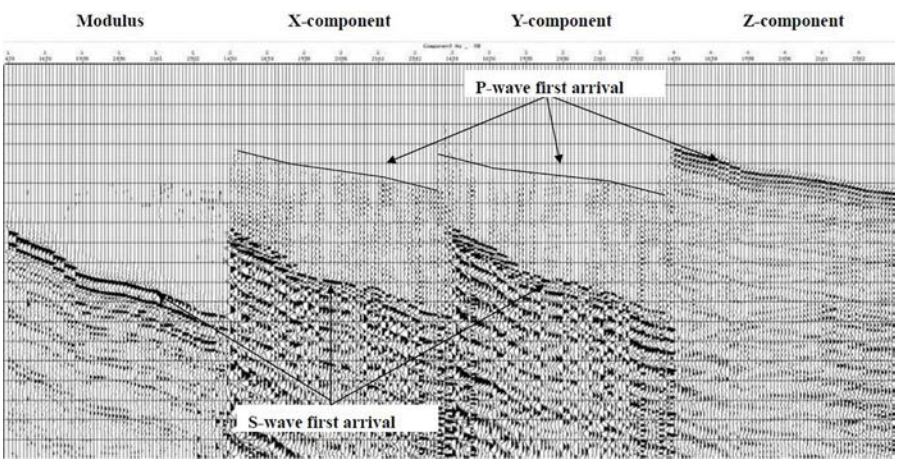

Figure 3.17 *From left to right Modulus, X, Y and Z-components before orientation. First arrival S-waves are clear on horizontal components while on the Z-component P-wave first arrivals are sharp to pick. The first arrival S-waves are not consistent before orientation while modulus (X^2 + Y^2) clearly shows the S-wave first arrivals. X, Y and Z components are displayed with the same constant gain while modulus has been normalized (after Kazemi, 2009).*

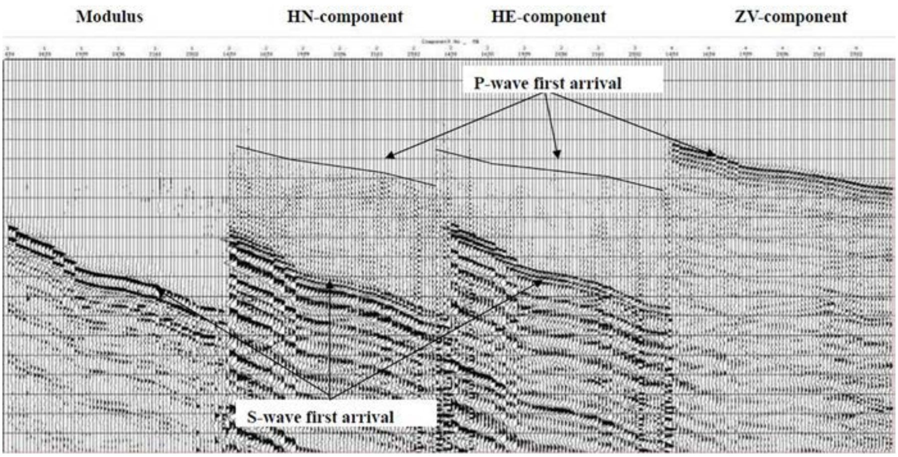

Figure 3.18 *From left to right Modulus, HN, HE and Z-components after orientation. On the Z-component P-wave first arrivals are sharp to pick. First arrival S-waves are coherent after orientation. The filtered modulus is identical before and after orientation. HN, HE and Z components are displayed in constant gain while modulus has been normalized. The modulus first arrivals are identical before and after orientation (after Kazemi, 2009).*

Naville et al. (2024a,b) shows an example of a 3C VSP obtained in the deviated section of the high-angle geothermal borehole of Grigny GGR5, targeting intra-Dogger thin, porous beds. Figure 3.19 shows the survey geometry and gives a summary of field parameters. One can notice the wide frequency bandwidth used for the vibrator sweep (5 to 175 Hz). Figure 3.20 shows the PP and PS VSP migrated sections. The reflectors surrounding the top Bathonian are slightly dipping to NE, and affected by several step faults, attenuated by lateral enhancement and migration. On the right side, the PS image converted to P-wave twt scale is restituted with higher definition due to the shorter shear wavelength. Main faults F1 & F2 are drawn on the bottom half of Figure 3.20, underlining lateral interruptions of reflectors. Many additional small faults are present on both PP and PS images (Naville et al., 2024a,b). To assist in a depth prediction of potential low velocity/high porosity target beds beneath the well, an inversion of the VSP PP-up image to acoustic impedance and acoustic velocity was performed. The inverted VSP sections highlight a depth interval of lower relative velocity and impedance at 1600–1612 m, which was revealed porous and productive (Figure 3.21).

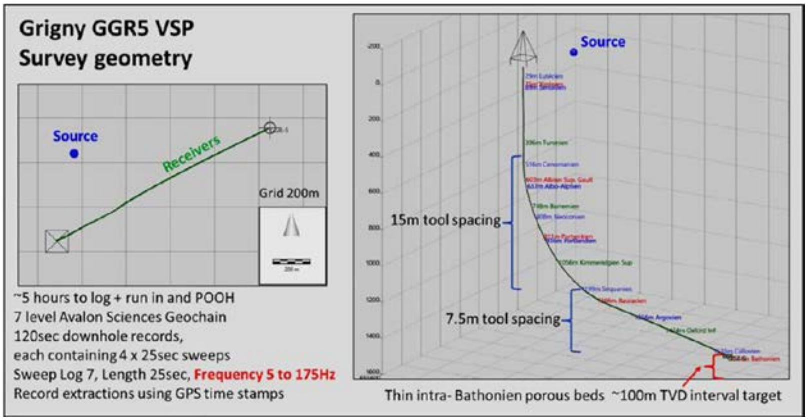

Figure 3.19 *GGR5-VSP, survey geometry, and summary of field parameters: plan view (left), 3D view (right) (after Naville et al., 2024a,b).*

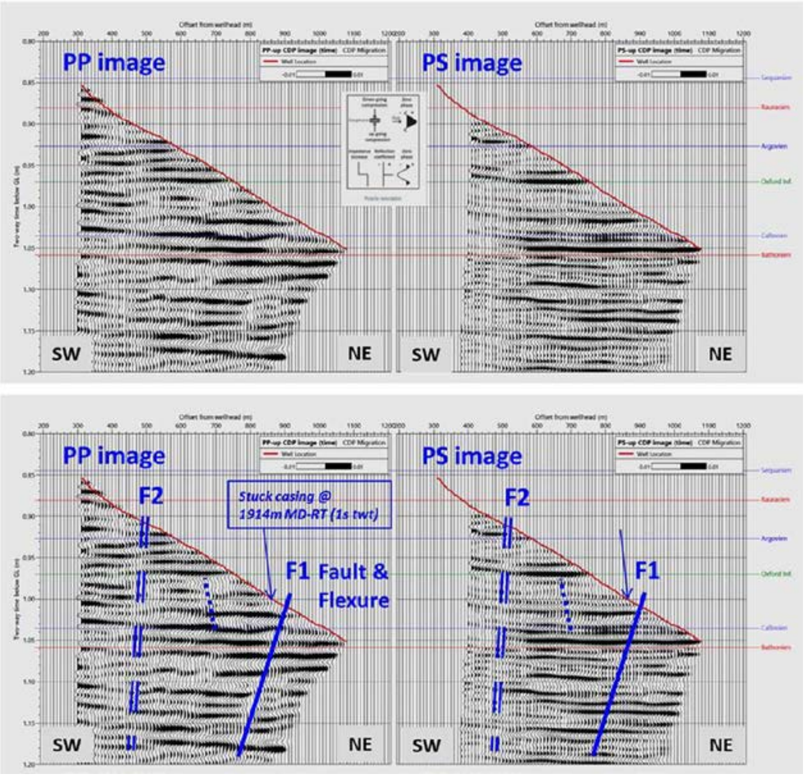

Figure 3.20 *PP-up and PS-up reflection images converted to time (twt). Main apparent faults are underlined on the bottom display, on both images (after Naville et al., 2024a,b).*

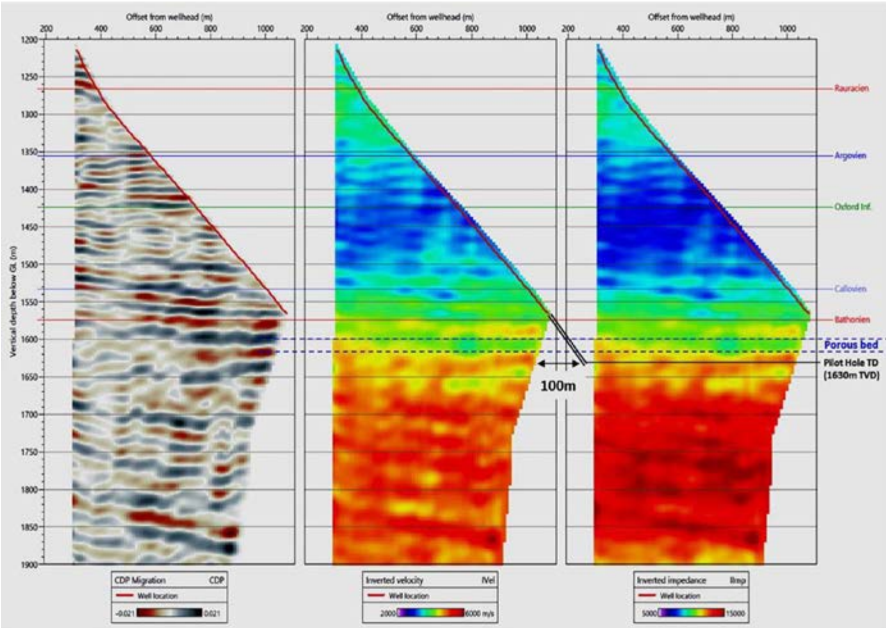

Figure 3.21 *PP-up image inverted, displayed in-depth scale. The VSP inversion predicted a porous zone below/ahead, which was confirmed by the pilot hole drilled after the VSP operation (after Naville et al., 2024a,b).*

Conclusion

Drilling of a borehole gives geophysicists the opportunity to perform borehole geophysical measurements and record additional data. Borehole geophysical methods can be classified as conventional logging methods, borehole surface imaging methods, hydrogeological logging methods, full waveform acoustic logging and borehole seismic methods such as VSP. Borehole geophysical methods provide high-resolution, localized information on rock properties like lithology, porosity, and fluid content. They also give borehole measurements used to validate and calibrate geophysical models, to convert in depth geophysical models obtained in time, to transform geophysical models into physical or petrophysical models.

With full waveform data, it is possible to conduct a well micro seismic survey based on the analysis of modes reflected and diffracted on acoustic impedance discontinuities within formations or at formation boundaries. Processing of reflected modes leads to depth acoustic sections with very high resolution (a few tens of centimeters) providing an image with a depth of investigation of several meters from the well trajectory. An example of depth acoustic section obtained in a highly deviated geothermal well shows the benefit of the acoustic method to detect stratigraphic structures observed within a potential geothermal reservoir

Offset 3C VSP data can be processed to obtain PP and PS migrated VSP sections, with a very high resolution. An example of a 3C VSP obtained in the deviated section of a geothermal borehole shows the detection of a low impedance thin layer (10 m thick) which was revealed porous and productive. VSP data, recorded with both a vertical geophone and a hydrophone, allows the detection of fluid waves and flows. As example, in a reconnaissance borehole drilled to determine the geothermal parameters of geological formations, the velocity and attenuation VSP logs show a very good correspondence with respect to the lithological variations observed in the borehole and confirm the presence of flows detected by a fluid wave. Furthermore, a good correspondence between the thermal conductivity profile and the attenuation VSP logs has been noticed.

The field examples show the benefit of using full waveform acoustic data and VSP, in addition to conventional and hydrogeological logs, for the characterisation of potential geothermal reservoirs.

References

The writing of the chapter (text and relative figures) is mainly based on the following papers and books.

Archie G.E. (1942) The electrical resistivity log as an aid in determining some reservoir characteristics, *Petroleum Technology* 1, 55-67.

Baird A., Vernier J., Goertz-Allmann B., Langet N., Rebel E., Wienecke S., Oates S. (2024) Improving the detection threshold of borehole DAS for seismic monitoring of CCS fields, paper 1367, 85th EAGE annual conference & exhibition, Oslo, Norway.

Bourbiaux B., Callot J.P., Doligez B., Fleury M., Gaumet F., Guiton M., Lenormand R., Mari J.L., Pourpak H. (2007) Multi-Scale Characterization of a Heterogeneous Aquifer through the Integration of Geological, Geophysical and Flow Data: A Case Study, *Oil and Gas Science and Technology, Rev IFP* 62, 347-373.

Boyer S., Mari J.L. (1997) *Seismic surveying and well logging*, Editions Technip, Paris.

Chapellier D. (2001a) Aquifer logging course, from On-line course of geophysics (http://www-ig.unil.ch/).

Chapellier D. (2001b) Petroleum logging course, from On-line course of geophysics (http://www-ig.unil.ch/).

Delay F., Mari J.L., Porel G., Chabaux F., Ackerer P. (2022) Is subsurface geophysics as seismic and acoustic investigations a rescue to groundwater flow inversion?, Comptes Rendus Geoscience, Part of Special Issue: Geo-hydrological data & models, https://doi.org/10.5802/crgeos.157.

Didraga C. (2015) DAS VSP recorded simultaneously in cemented and tubing installed fiber optic cables, TU N11814, 77th EAGE annual conference & exhibition, IFEMA Madrid, Spain.

Faust L.Y. (1953) A velocity function including lithologic variation, *Geophysics* 18, 271-288.

Gaillard T., Moreau M., Mari J.L. (2024) Seismic and stratigraphic characterization of karstogenic horizons in a sequence of carbonate deposits: Example of the Dogger limestones of the Poitou threshold, Journees Scientifiques AGAP Qualité 2024, E3S Web of Conferences 504, 05005, https://doi.org/10.1051/e3sconf/202450405005

Hardage B.A. (1985) *Vertical seismic profiling*, Part A: principles, Part B: advanced concepts, Geophysical Press, London.

Hardage B.A. (1992) *Cross well Seismology and Reverse VSP*, Geophysical Press, London.

Hirabayashi N., Dahlhaus L., Kumar R., Jocker J., Wielemaker E., Khaitan M.L., Naville C. (2024) Analysis of geologic structures using deep sonic imaging, in International Meeting for Applied Geoscience & Energy, https://doi.org/10.1190/image2024-4091360.1.

Kazemi K. (2009) Seismic imaging of thrust fault structures in Zagros Iranian oil fields, from surface and well data, PhD, Université de Cergy-Pontoise, https://hal.inria.fr/file/index/docid/414628/filename/Thesis_kazemi.pdf.

Lesnikov V., Allanic C. (2014) DAS VSP acquisition: perspective and challenges, WS15-D01, 76th EAGE annual conference & exhibition, Amsterdam RAI, The Netherlands.

Mari J.L. (1989) Q-log determination on downgoing wavelets an tube wave analysis in vertical seismic profiles, *Geophysical prospecting* 37(3), 257-277, https://doi.org/10.1111/j.1365-2478.1989.tb02206.x.

Mari J.L. (2015) *Signal processing for geologists & geophysicists*, e-book, http://books.ifpenergiesnouvelles.fr/ebooks/signal-processing.

Mari J.L., Coppens F. (2003) Well seismic surveying, Éditions Technip, Paris, ISBN 2-7108-076-9, ISSN 1271-9048.

Mari J.L., Delay F. (2024) Stoneley wave detection by acoustic interferometry: Estimation of shear velocity of a geological formation, Journees Scientifiques AGAP Qualité 2024, E3S Web of Conferences 504, 02004, https://doi.org/10.1051/e3sconf/202450402004.

Mari J.L., Porel G. (2007) 3D seismic imaging of a near – surface heterogeneous aquifer: a case study, *Oil and Gas Science and Technology, Rev IFP* 63, 179-201, https://doi.org/10.2516/ogst:2007077.

Mari J.L., Porel G. (2024) The hydrogeological experimental site of Poitiers: Hydrogeological versus geophysical investigations, Journees Scientifiques AGAP Qualité 2024, E3S Web of Conferences 504, 05003, https://doi.org/10.1051/e3sconf/202450405003.

Mari J.L., Vergniault C. (2018) *Well seismic surveying and acoustic logging*, EDP-Sciences, https://doi.org/10.1051/978-2-7598-2263-8.

Mari J.L., Arens G., Chapellier D., Gaudiani P. (1999) *Geophysics of reservoir and civil engineering*, Editions Technip, Paris, ISBN 2-7108-0757-2.

Mari J.L., Delay F., Porel G., Gaudiani P. (2021) Characterizing flow in the first hundred-meter depth of a fractured aquifer using hybrid seismic methods, acoustic logging, and flow log measurements, *Oil & Gas Science and Technology, Rev. IFP Energies Nouvelles* 76, 62, https://doi.org/10.2516/ogst/2021048.

Mari J.L., Delay F., Voisin C., Gaudiani P. (2023) Active and passive acoustic logging applied to the detection of preferential flow in a sedimentary aquifer, Science and Technology for Energy Transition, https://doi.org/10.2516/stet/2023018.

Mari J.L., Mendes M. (2019) *Seismic imaging: a practical approach*, EDP Sciences, https://www.edp-open.org/seismic-imaging-a-practical-approach.

Mari J.L, Münzberger P., Colbach R., Peignard L., Al Khatib H. (2024) Contribution of 2-component VSP measurements to the characterization of a geothermal site, paper 715, 85th EAGE annual conference & exhibition, Oslo, Norway.

Mari J.L., Porel G., Delay F. (2020) Contribution of Full Wave Acoustic Logging to the Detection and Prediction of Karstic Bodies, *Water* 12(4), 948, https://doi.org/10.3390/w12040948.

Mars J., Glangeaud F., Boelle J.L., Vanpe J.M. (1999) Wave separation by an oblique polarization filter, PSIPP'99, First international symposium on Physics in Signal and Image Processing, 18- 19 January 1999, Paris, France, 94-108.

Mateeva A., Lopez J., Mestayer J., Wills P., Kiyashchenko D., Yang Z., Berlang W., Detomo R., Grandi S. (2013) Distributed acoustic sensing for reservoir monitoring with VSP, *The Leading Edge* 32, 1278-1283.

Mateeva A., Lopez J., Potters H., Mestayer J., Cox B., Kiyashchenko D., Wills P., Grandi S., Hornman K., Kuvshinov B., Berlang W., Yang Z., Detomo R. (2014) Distributed Acoustic Sensing for reservoir monitoring with Vertical Seismic Profiling, *Geophysical Prospecting* 62, 679-692.

Mestayer J., Cox B., Wills P., Kiyashchenko D., Lopez J., Costello M., Bourne S., Ugueto G., Lupton R., Solano G., Hill D., Lewis A. (2011) Field trials of distributed acoustic sensing for geophysical monitoring, 81st SEG Annual International Meeting, Expanded Abstracts.

Naville C. (2024) IFPEN-APS-PPZG: Orientation of 3 component rig source VSPs, in IFPEN Online presentation, https://www.ifpenergiesnouvelles.fr/breve/ifpen-aps-ppzg-orientation-3-component-rig-source-vsps.

Naville C., Bailey J., Humphries M., Vicelli J., Hanot F. (2024a) HF/HR VSP acquisition processing, and interpretation in the deviated section of the high angle geothermal borehole of Grigny GGR5, targeting intra Dogger thin, porous beds, Science and Technology for Energy Transition, https://doi.org/10.2516/stet/2024051.

Naville C., Soulas S., Antics M., Ungemach P. (2024b) Illustration of a land VSP field operation with vibrator source around the drilling site, Grand Paris area, France, in Researchgate, https://doi.org/10.13140/RG.2.2.10611.09765.

Raymer L.L., Hunt E.R., Gardner J.S. (1980) An improved sonic transit time to porosity transform. Trans. SPWLA 21st Annual Logging Symposium, July 8-11, 1980, 1-12.

Rosenbaum J.H. (1974) Synthetic microseismograms: logging in porous formation, *Geophysics* 39, 14-32.

Serbutoviez S., Naville C., Throo A., Bruneau J. (2003) 3C VSP Processing and Interpretation, in IFPEN Online presentation, November 2003, revised July 2020, https://www.ifpenergiesnouvelles.com/sites/ifpen.fr/files/inline-images/NEWSROOM/Actualit%C3%A9s/2020-True%20Amplitude%203C-VSP-method.pdf.

Serra O., Serra L. (2000) *Diagraphies, Acquisition et applications*, Editions Serralog, ISBN: 9782951561601.

Willis M.E. (2022) Distributed Acoustic Sensing for Seismic Measurements – What Geophysicists and Engineers Need to Know, Society of Exploration Geophysicists: Houston, TX, USA, pp. 45–52 https://doi.org/10.1190/1.9781560803850.

Wyatt K.D., Wyatt S.B. (1982) Determination of subsurface structural information using the vertical seismic profile, *Geophysics* 47(7), 1123-1128.

Wyllie M.R.J., Gregory A.R., Gardner L.W. (1956) Elastic wave velocities in heterogeneous and porous media, *Geophysics* 21, 41-70.